ACADÉMIE
DES SCIENCES
INSTITUT DE FRANCE

Comptes Rendus
Physique

Sylvain Nascimbene

Simulating quantum Hall physics in ultracold atomic gases: prospects and challenges

Volume 26 (2025), p. 317-338

Online since: 26 March 2025

https://doi.org/10.5802/crphys.243

The Comptes Rendus. Physique *are a member of the Mersenne Center for open scientific publishing*
www.centre-mersenne.org — e-ISSN : 1878-1535

ACADÉMIE DES SCIENCES
INSTITUT DE FRANCE

Comptes Rendus. Physique
2025, Vol. 26, p. 317-338
https://doi.org/10.5802/crphys.243

Intervention in a conference / *Intervention en colloque*

Simulating quantum Hall physics in ultracold atomic gases: prospects and challenges

Simuler l'effet Hall quantique dans les gaz d'atomes ultrafroids : perspectives et défis

Sylvain Nascimbene [a]

[a] Laboratoire Kastler Brossel, Collège de France, CNRS, ENS-PSL University, Sorbonne Université, 11 Place Marcelin Berthelot, 75005 Paris, France

E-mail: sylvain.nascimbene@lkb.ens.fr

Abstract. This proceedings presents recent advancements in the realization of topological states of matter using ultracold atomic gases. We focus on the simulation of the quantum Hall effect, originally discovered in two-dimensional electron gases subjected to a magnetic field. Given that ultracold atoms are neutral, simulating the effect of a magnetic field requires an ad-hoc technique. We review various methods developed for this purpose, highlighting their respective advantages and limitations. Furthermore, we explore the extension of these techniques to interacting quantum gases within topological bands, aiming to create analogs of fractional quantum Hall states. These many-body states are distinguished by their topological order, which is characterized by long-range entanglement among particles and the emergence of low-lying excitations exhibiting fractional quantum statistics. The discussion will encompass the current state of research and potential future directions in the field.

Résumé. Cet acte de congrès présente les avancées récentes dans la réalisation d'états topologiques de la matière à l'aide de gaz atomiques ultrafroids. Nous nous concentrons sur la simulation de l'effet Hall quantique, découvert dans des gaz d'électrons bidimensionnels soumis à un champ magnétique. Étant donné que les atomes ultrafroids sont neutres, la simulation de l'effet d'un champ magnétique nécessite une technique ad hoc. Nous passons en revue diverses méthodes développées à cette fin, en soulignant leurs avantages et leurs limites respectifs. En outre, nous explorons l'extension de ces techniques aux gaz quantiques en interaction dans des bandes topologiques, dans le but de créer des analogues d'états de Hall fractionnaires. Ces états à N corps se distinguent par leur ordre topologique, qui se caractérise par une intrication à longue portée entre les particules et l'émergence d'excitations de basse énergie présentant des statistiques quantiques fractionnaires. La discussion portera sur l'état actuel de la recherche et sur les orientations futures potentielles dans ce domaine.

Keywords. Topological phase, Quantum simulation, Quantum gases.

Mots-clés. Phase topologique, Simulation quantique, Gaz quantiques.

Funding. European Union (grant TOPODY 756722 from the European Research Council), Institut Universitaire de France.

Manuscript received 17 September 2024, revised 12 February 2025, accepted 24 February 2025.

The quantum Hall effect was discovered in 1980 by von Klitzing [1] by studying the properties of condensed-matter systems in which the electron gas is constrained to evolve in a

two-dimensional (2D) plane xy. At low temperature and in the presence of a strong magnetic field $\mathbf{B} = B\mathbf{e}_z$, he observed a quantization of the Hall conductance according to

$$I_y = \sigma_{xy} V_x, \quad \sigma_{xy} = n\sigma_0,$$

where n is an integer, $\sigma_0 = e^2/h$ is the quantum of conductance, with e representing the electron charge and h the Planck constant. This discovery was pivotal in the field of quantum many-body physics and laid the groundwork for the exploration of topological states of matter. We will discuss here the current state of research in ultracold atomic gases towards the simulation of the quantum Hall effect and the realization of various topological states of matter associated with it.

1. Topological bands and the integer quantum Hall effect

1.1. *Landau levels*

The integer quantum Hall effect can be understood in terms of a special topological structure of single-particle quantum eigenstates of motion. Before delving into more complex systems, we examine the idealized model of a charged particle evolving in 2D and subjected solely to a perpendicular magnetic field [2]. Its dynamics is determined by the Hamiltonian

$$H = \frac{(\mathbf{p} - q\mathbf{A})^2}{2M},$$

where q is the particle charge ($-e$ for an electron, but in the subsequent discussion we will assume $q > 0$) and M is its mass. The selection of the gauge influences the inherent symmetries of the system. In our discussion, we will primarily utilize the symmetric gauge, defined as

$$\mathbf{A} = \frac{1}{2}\mathbf{B} \times \mathbf{r} = \frac{Br}{2}\mathbf{e}_\phi.$$

While this choice explicitly breaks translational invariance, it preserves rotational symmetry around the origin.

The Hamiltonian can be expanded as

$$H = H_0 - \frac{\omega_c}{2} L_z, \tag{1}$$

$$H_0 = \frac{p_x^2 + p_y^2}{2M} + \frac{1}{8} M\omega_c^2 (x^2 + y^2), \tag{2}$$

where we introduce the cyclotron frequency $\omega_c = qB/M$ and the angular momentum projection $L_z = xp_y - yp_x$. The Hamiltonian H_0 corresponds to an isotropic harmonic oscillator in 2D, of frequency $\omega_c/2$. We can exhibit an eigenbasis $|n_0, m\rangle$ of H_0 in common with the angular momentum L_z, corresponding to the energy spectrum $E^0_{n_0,m} = (n_0 + 1)(\hbar\omega_c/2)$ where $n_0 \in \mathbb{N}$ and $m \in \{-n_0, -n_0 + 2, \ldots, n_0 - 2, n_0\}$ (see Figure 1(a)).

Together with the term $(-\omega_c/2)L_z$, we get the energy spectrum of a charged particle in a magnetic field $E_{n_0,m} = E^0_{n_0,m} - m(\hbar\omega_c/2)$, which can be written as

$$E_{n,m} = (n + \tfrac{1}{2})\hbar\omega_c,$$

with $n = (n_0 - m)/2 \in \mathbb{N}$ and $m \geq -n$. The energy spectrum consists of infinitely degenerate flat bands known as Landau levels, as illustrated in Figure 1(b).

In the following we will focus on properties of the ground band, the lowest Landau level (LLL). Its eigenstates are described by the wavefunctions

$$\psi_m(x, y) \propto r^m e^{im\phi} e^{-r^2/4\ell^2},$$

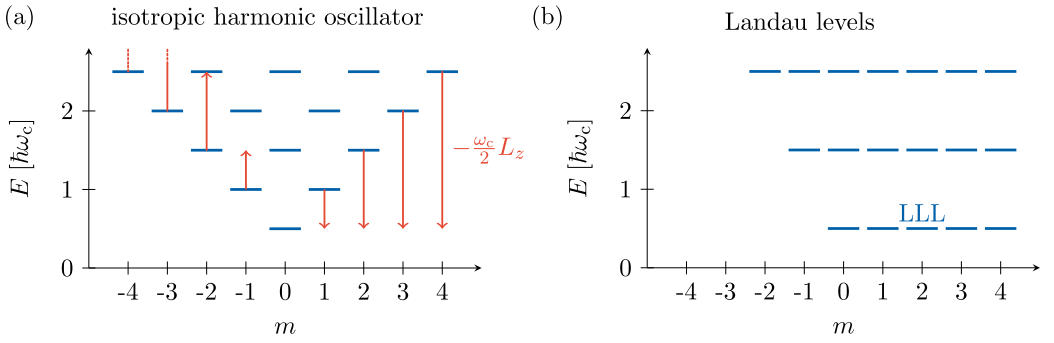

Figure 1. (a) Spectrum of the isotropic quantum harmonic oscillator in two dimensions. Offseting the states by $-(\omega_c/2)L_z$ (red arrows) yields the spectrum of a charged particle subjected to a magnetic field, corresponding to Landau levels shown in (b).

where $m \geq 0$. Here, we introduced the polar coordinates (r,ϕ) and the cyclotron length $\ell = \sqrt{\hbar/qB}$. The density probability of ψ_m is concentrated in a ring of radius $r_m \simeq \sqrt{2m}\ell$, of width $\Delta r \simeq \ell$ independent of m. The area enclosed by this ring is thread by a magnetic flux

$$\Phi_m = B\pi r_m^2 \simeq m\Phi_0,$$

where $\Phi_0 = h/q$ is the magnetic flux quantum.

In the following, we will consider a finite geometry, assuming that the motion is restricted to a disk $r \leq R$ by a circular hard wall. This restriction only weakly affects the so-called bulk states ψ_m with $r_m \leq R$ (i.e. $m \leq m_{\max} = R^2/2\ell^2$) for which the density probability is almost fully contained within the disk. For $m \geq m_{\max}$, the eigenstates become squeezed by the confinement hard wall close to $r = R$, leading to an increase of (kinetic) energy (see Figure 2(a)). As a result, these states acquire a non-zero azimuthal velocity $\langle v_\phi \rangle$, in contrast with the dispersionless bulk modes. More precisely, we write the azimuthal velocity component as

$$\begin{aligned} v_\phi &= \frac{1}{M}\left(\frac{\hbar}{\mathrm{i}r}\partial_\phi - qA_\phi\right) \\ &= \frac{1}{M}\left(\frac{\hbar m}{r} - \frac{qB}{2}r\right) \\ &= \omega_c \frac{r_m^2 - r^2}{r}. \end{aligned}$$

For bulk states, the azimuthal velocity almost vanishes since $r \simeq r_m$. Conversely, for edge modes the density is localized around $r = R$, hence $v_\phi \propto (r_m^2 - R^2) \propto (m - m_{\max})$, corresponding to a chiral dispersive mode [3] (see Figure 2(b)).

Introducing the complex coordinate $z = re^{\mathrm{i}\phi} = x + \mathrm{i}y$, a generic bulk state of the Landau level can be expanded over the ψ_m basis as

$$\psi(z) = \sum_{m\geq 0}^{m_{\max}} c_m z^m \mathrm{e}^{-r^2/4\ell^2},$$

which is the product of a gaussian factor in r and a complex polynomial $P(z)$. This polynomial is fully characterized by its roots z_k, as

$$P(z) \propto \prod_{k=1}^{m_{\max}} (z - z_k).$$

One checks that the complex phase of $P(z)$ winds once around every non-degenerate root z_k, corresponding to a unit-charge quantum vortex.

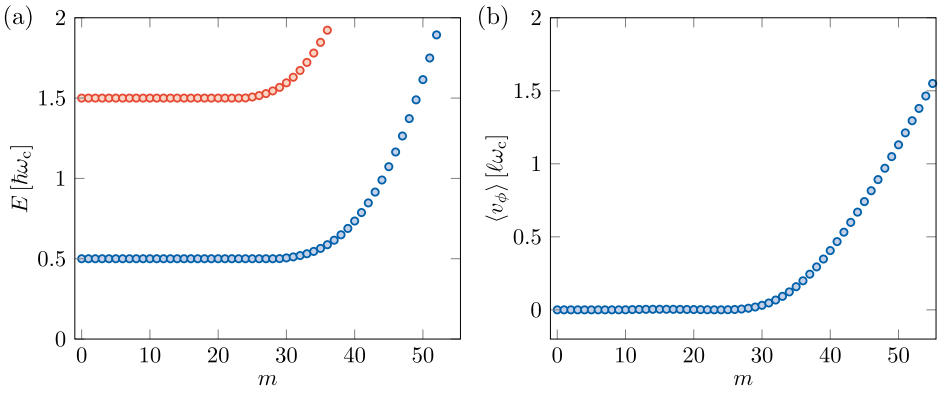

Figure 2. (a) Spectrum of a quantum Hall system restricted to a disk for radius $R = 10\ell$. (b) Mean azimuthal velocity for the quantum states of the ground energy band.

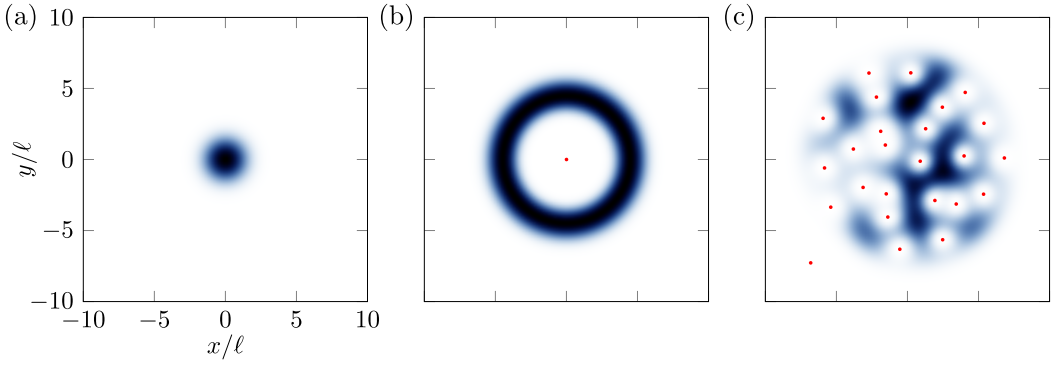

Figure 3. Probability density distribution of a few states of the LLL: the state $\psi_{m=0}$ (a), the state $\psi_{m=10}$ (b), and a state defined by a random complex polynomial of degree 25 (c). Vortex point defects are shown as red dots.

We show in Figure 3 the density probability of a few typical states of the LLL, namely $\psi_{m=0}$, $\psi_{m=10}$, and a state defined by a random complex polynomial of degree 25, which could be realized using a thermal Bose gas restricted to the LLL [4]. We also show for each of them the position of the quantum vortices as red dots.

1.2. *Quantization of the Hall conductance*

The first explanation of the Hall conductance quantization was given by Laughlin based on a particle pumping argument [5]. For this, we consider a slightly modified geometry, coined Corbino disk $r_{\rm min} \le r \le r_{\rm max}$ [3,6] (see Figure 4(a)). In a fermionic band insulator, the states with

$$m_{\rm min} = \frac{r_{\rm min}^2}{2\ell^2} \le m \le m_{\rm max} = \frac{r_{\rm max}^2}{2\ell^2}$$

are occupied with one particle. We consider a solenoid, placed within the inner radius, which can introduce an additional magnetic flux Φ. By slowly increasing this flux by one unit of flux quantum Φ_0, the adiabatic eigenstates undergo a spectral flow in which the state ψ_m (which originally encloses a magnetic flux $m\Phi_0$) is transferred to the next state ψ_{m+1} (enclosing a

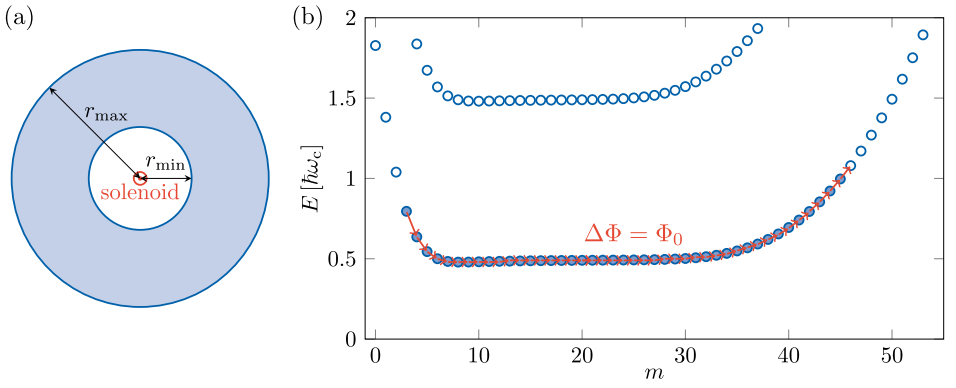

Figure 4. (a) Scheme of the Corbino disk used for Laughlin's pump experiment. (b) Single-particle spectrum of a Corbino disk defined by the radii $r_{\min} = 2\ell$ and $r_{\max} = 10\ell$. Starting in a fermionic insulator with a Fermi level $E_F = \hbar\omega_c$, the adiabatic increase of the solenoid flux $\Delta\Phi = \Phi_0$ transfers each state m to $m+1$ (red arrows), or equivalently a state from one edge to the other.

magnetic flux $(m+1)\Phi_0$). Globally, such a pump cycle transfers one particle from the inner edge (state $m_{\min}$) to the outer edge (state $m_{\max}$), as shown in Figure 4(b).

This pump process can be interpreted in terms of a quantized Hall conductance. Indeed, the flux variation $\dot{\Phi}$ gives rise to an "induced voltage" $V_\phi = -\dot{\Phi}$ along any circular path within the Corbino disk, while the transfer of particles from the inner to outer edges can be interpreted as a radial current

$$I_r = q\frac{\dot{\Phi}}{\Phi_0} = -\frac{q^2}{h}V_\phi.$$

This relationship aligns with the quantization of the Hall conductance.

1.3. *Topological bands in lattice systems*

The quantization of Hall conductance is not limited to ideal Landau levels; it can also be extended to Bloch bands in lattice systems.

We begin by examining the natural extension of Landau levels to a discrete square lattice, known as the Hofstadter model [7,8]. This model features a square lattice with nearest-neighbor hopping, where the positions of the lattice sites are defined as $\mathbf{r}_{i,j} = i\,a\mathbf{e}_x + j\,a\mathbf{e}_y$, where a is the lattice spacing and i, j are integers. In this framework, the magnetic field is incorporated through the Peierls substitution, which introduces complex phases into the hopping amplitudes. These phases correspond to the Aharonov–Bohm phase acquired along the path connecting neighboring sites. To simplify the description, we adopt the Landau gauge, where $A_x = -By$. In this gauge, the hopping terms along the y-direction remain real, while the hopping terms along the x-direction acquire a Peierls phase given by

$$\phi_{(i,j)\to(i+1,j)} = \frac{q}{\hbar}\int_{\mathbf{r}_{i,j}}^{\mathbf{r}_{i+1,j}} \mathrm{d}\mathbf{r}\, A_x(\mathbf{r}) = -2\pi\frac{\Phi}{\Phi_0}j, \tag{3}$$

where $\Phi = Ba^2$ is the magnetic flux through a unit cell.

In the general case, the position-dependent Peierls phases disrupt translational symmetry along the y-direction, making it impossible to define y-momentum. However, when the ratio Φ/Φ_0 takes on rational values p/q, discrete translation invariance by the distance qa along y is recovered (in addition to the discrete invariance along x by the distance a). As a result, one

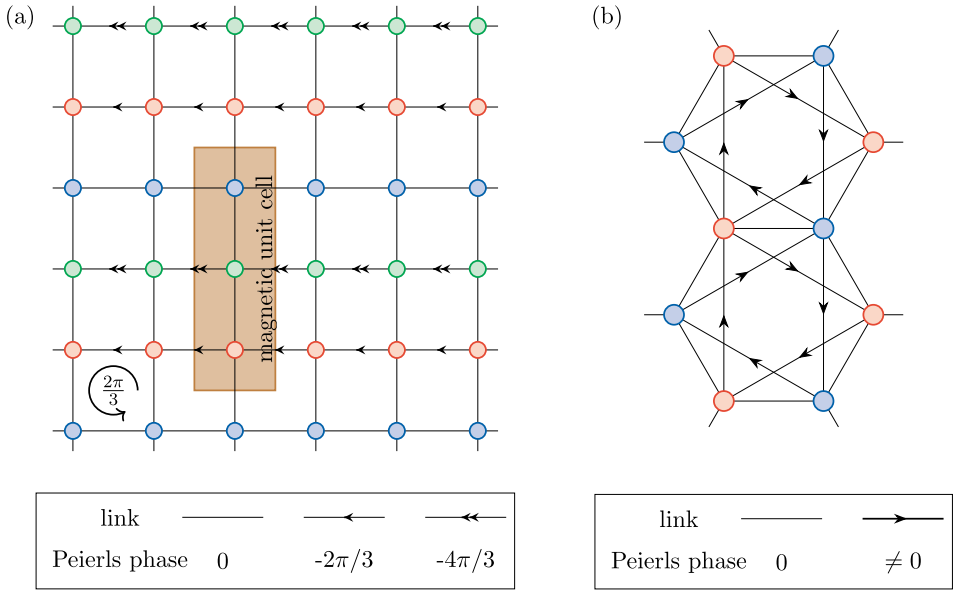

Figure 5. (a) Scheme of the Hofstadter model, a square lattice model with complex-valued hopping matrix elements as defined in Equation (3). For a ratio $p/q = 1/3$, the lattice exhibits three inequivalent sites and a magnetic Brillouin zone defined by three square unit cells. (b) Scheme of the Haldane model, a hexagonal lattice model with real-valued nearest-neighbour hoppings and complex-valued next-nearest neighbour hoppings.

can introduce a conserved quasi-momentum (q_x, q_y) defined over a magnetic Brillouin zone $(0, 2\pi/a) \times (0, 2\pi/qa)$ (see the case $p/q = 1/3$ in Figure 5(a)).

As a result of the magnetic translation symmetries discussed above, quantum levels are organized into a set of q magnetic Bloch bands. A given band, provided it is separated in energy from other bands, gives rise to a quantized Hall effect. Each band, when sufficiently separated in energy from others, can give rise to a quantized Hall effect. Specifically, the transverse linear response of a band insulator manifests as a quantized Hall conductance expressed by $\sigma_{xy} = \mathscr{C}\sigma_0$, where $\mathscr{C}$ is an integer known as the Chern number. This integer characterizes the topological properties of the Bloch band, analogous to the genus of a closed surface in geometry. For instance, in the case where $p = 1$, the lowest Bloch band consistently exhibits a Chern number of $\mathscr{C} = 1$, resembling the behavior of a Landau level. We do not discuss here the concept of Chern number in more detail, since it is very well explained in several review articles (see for example [9] for a review in a context of ultracold quantum gases).

The concept of the Chern number is not confined to lattice models that can be viewed as discretized versions of continuous systems with uniform magnetic fields. It can be defined for any isolated Bloch band within a given lattice model. A Chern insulator emerges when fermionic insulators fill Bloch bands that possess a non-zero Chern number, which requires that the configuration of Peierls phases breaks time-reversal symmetry. A notable example of a Chern insulator is the Haldane model [10], illustrated in Figure 5(b).

2. Realizing quantum Hall systems with ultracold atoms

Since magnetic fields do not exert mechanical effects on neutral particles, simulating quantum Hall physics relies on analogies. In this section, we will review some of these analogies, discuss

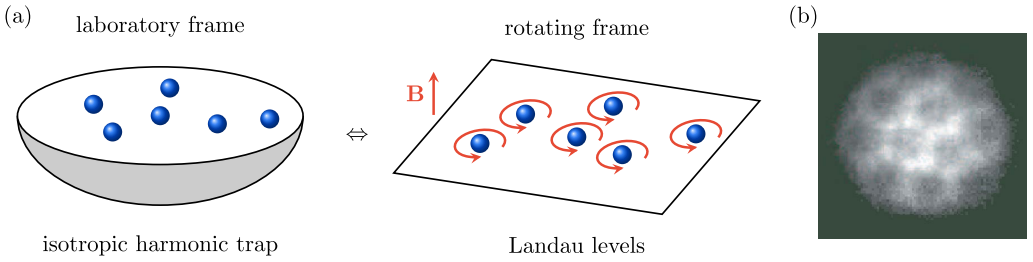

Figure 6. (a) Schematics of the analogy between an atom held in an isotropic harmonic trap in a rotating frame and a charged particle subjected to a magnetic field. (b) Image of an atomic Bose–Einstein condensate set in rotation, which exhibits a triangular lattice of quantized vortices (from [12]).

their current limitations, and explore potential strategies to overcome these challenges in the future.

2.1. *Rotating gases*

2.1.1. *Landau levels in rotating gases*

Historically, the first protocol to create an effective magnetic field involves rotating gases [11]. Consider an atom evolving in two dimensions under an isotropic harmonic trap, described by the Hamiltonian

$$H = \frac{p_x^2}{2M} + \frac{p_y^2}{2M} + \frac{1}{2}M\omega^2(x^2+y^2).$$

In a reference frame that rotates around the center of the harmonic trap at a frequency Ω, the Hamiltonian transforms to

$$H' = \frac{\mathbf{p}'^2}{2M} + \frac{1}{2}M\omega^2\mathbf{r}'^2 - \Omega L_z',$$

where $L_z' = x'p_y' - y'p_x'$ is the angular momentum and (x', y') are the rotated coordinates. When the rotation frequency Ω matches the confinement frequency ω, we recover the Landau Hamiltonian given in Equation (1), corresponding to a particle of charge $q = 1$ and a cyclotron frequency $\omega_c = 2\omega$ (see Figure 6(a)).

2.1.2. *Abrikosov vortex lattices in Bose–Einstein condensates*

Most experiments with rotating gases have focused on Bose–Einstein condensates containing a large number of atoms N. These systems can be effectively described by a classical field $\psi(x, y)$ representing the macroscopic wavefunction shared by all atoms. As previously discussed, a generic wavefunction in the LLL is characterized by its zeros, which correspond to unit-charged quantum vortices.

In the absence of interactions, any configuration of vortices can be expected due to the flat-band nature of the LLL. However, interactions lead to a well-defined many-body ground state. In dilute gases, atoms primarily interact at short range, resulting in a ground state that minimizes the interaction energy [13]

$$E_{\text{int}} = g\frac{N(N-1)}{2}\int \mathrm{d}r^2\,|\psi(r)|^4,$$

where g is the interaction coupling constant. Without a magnetic field, such as in a free Bose gas within a box potential of area $\mathscr{A}$, the energy is minimized with a uniform density $n = |\psi|^2 = N/\mathscr{A}$ (ignoring boundary effects). When a magnetic field is applied, distributing the density over

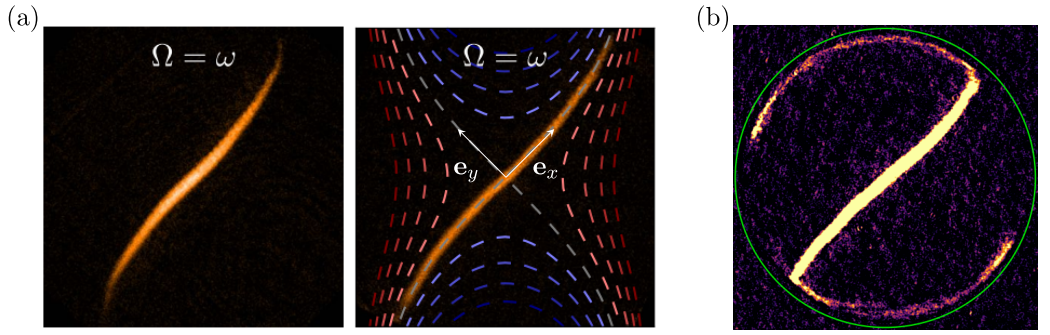

Figure 7. (a) In situ image of an atomic gas in the momentum state $p_x = 0$ of the LLL (from [18]). The right panel indicates as dashed lines the equipotential lines of the rotating saddle potential. (b) In situ image of the atomic gas in the presence of a sharp circular box potential (green circle). The atoms populate a chiral edge mode propagating along the boundary (from [19]).

the area $\mathscr{A}$ necessitates the insertion of $N_\Phi = B\mathscr{A}/\Phi_0$ quantum vortices. As shown in [14], the interaction energy is minimized with a regular arrangement of vortices in a triangular lattice.

Vortex lattices have been realized and extensively studied in the early years of atomic BECs, although most cases did not restrict to the LLL (see Figure 6(b)) [11,15–17]. However, exploring quantum Hall physics through rotating gases presents significant challenges, as these systems are highly sensitive to any static defect potential in the lab frame, which induces time-dependent perturbations in the rotating frame.

2.1.3. *Recent experiments in the LLL*

Recent experiments conducted by the group of Zwierlein have rekindled interest in rotating gases [18]. Compared to experiments from the 2000s, these new studies benefit from advanced techniques such as high-resolution in situ imaging and potential imprinting. This allows fine potential defect diagnosis, as well as the capability to project a hard-wall potential, enabling the investigation of uniform gases in a circular box. The rotation was induced by a rotating quadrupolar potential given by $V(x,y) = -Qxy$ with $Q > 0$, as illustrated in Figure 7(a) (we will omit the prime notation in the following discussion).

The dynamics induced by the saddle potential can initially be understood through classical orbits. In the lowest Landau level, the slow motion of atoms—characterized by the drift of guiding centers of cyclotron orbits—is governed by the equation of motion

$$\mathbf{v} = \frac{1}{q}\frac{\nabla V \times \mathbf{B}}{B^2},$$

which simplifies here to

$$\mathbf{v} = \frac{Q}{2M\omega}(x\mathbf{e}_x - y\mathbf{e}_y).$$

Starting from a rotationally symmetric Gaussian distribution, we expect the gas to contract along the y-direction while elongating along the x-direction. Eventually, the extent along y saturates at the cyclotron length ℓ, beyond which classical dynamics ceases to apply.

This dynamics accounts for the formation of a highly elongated gas in the MIT experiments, as illustrated in Figure 7(a). This state can be interpreted as the occupation of a well-defined wavefunction from the LLL, specifically a momentum state expressed in the Landau gauge $\mathbf{A} = -By\mathbf{e}_x$.

In this gauge, rotational symmetry is broken, and the system exhibits continuous translation symmetry along the x-direction. The Hamiltonian is given by

$$H = \frac{(p_x + qBy)^2}{2M} + \frac{p_y^2}{2M},$$

where the momentum p_x acts as a fixed parameter, resulting in a one-dimensional harmonic oscillator along y. The LLL, parameterized by p_x, corresponds to the ground state:

$$\psi_{p_x}(x,y) = \mathrm{e}^{\mathrm{i}p_x x/\hbar} \exp\left[-\frac{(y - p_x \ell^2/\hbar)^2}{2\ell^2}\right].$$

Returning to the MIT experiments, the elongated gas is very close to the state $p_x = 0$[1].

The control of rotating gases at the level of a single LLL wavefunction laid the groundwork for subsequent experiments, where the population of chiral edge modes localized near the boundary of a sharp box potential was observed (see Figure 7(b)) [19]. Additionally, the effects of interactions in the flat-band limit were investigated, revealing a redistribution of momentum within the LLL due to interactions, which led to vortex crystallization as a precursor to the formation of an Abrikosov lattice [20].

2.2. *Lattice systems*

2.2.1. *Peierls phase engineering*

Atomic gases in optical lattices provide a versatile platform for simulating a wide range of discrete lattice models [21]. Here, we focus on the realization of lattices with non-trivial topological bands, which require complex-valued hopping amplitudes. In a standard optical lattice created by the dipole trapping of an off-resonant standing wave, atoms hop through spontaneous tunneling events characterized by real-valued transition amplitudes. The proposal by Jaksch and Zoller [22] established the framework for simulating Peierls phases.

We present a simplified version of this scheme that aligns more closely with actual experimental implementations. By introducing a linear potential, we create an energy offset $\hbar\Delta$ between neighboring wells along the x-direction, effectively suppressing tunneling (see Figure 8(a)). The x-dynamics can be restored by employing a pair of laser beams to induce a two-photon optical transition.

The hopping amplitude inherits the electric field amplitudes $E_1 E_2^* \propto \mathrm{e}^{\mathrm{i}\delta\mathbf{k}\cdot\mathbf{r}}$, where $\delta\mathbf{k}$ represents the relative light momentum. The complex phases of these amplitudes function as the Peierls phases associated with a magnetic field, yielding a flux per plaquette given by

$$\Phi = \Phi_0 \frac{\delta k_y a}{2\pi}.$$

Since the lattice spacing a is comparable to the laser wavelength, the flux is typically on the order of 1 and can be adjusted by modifying the lattice geometry or the angle between the two driving beams. This scheme, along with similar protocols, has been successfully implemented to simulate both the Hofstadter and Haldane models discussed in Section 1.3 [23,25,26].

2.2.2. *Probing the band topology*

Various protocols have been developed to probe band topology (see [9] for a review). Here, we focus on one such method that examines the transverse linear response of an atomic gas evolving under the Hofstadter model with a flux $p/q = 1/4$ [24]. Instead of filling the lowest energy band with a fermionic band insulator, a thermal Bose gas samples the ground band uniformly and

[1] The momentum state $p_x = 0$ is the only momentum state unaffected by the saddle potential.

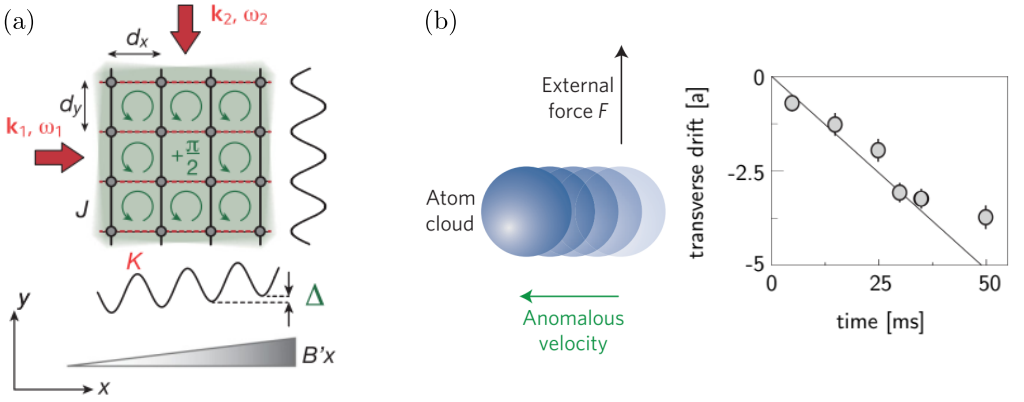

Figure 8. (a) Scheme of the lattice configuration and shaking protocol used to engineer the Hofstadter model with a magnetic flux $p/q = 1/4$ (from [23]). A linear potential induced by a magnetic field gradient suppresses tunneling along the x-direction. A pair of Bragg laser beams induces resonant tunneling along x, imprinting the complex phase profile of the Bragg process onto the hopping matrix elements. (b) Scheme of the transverse Hall response measurements and measured Hall drift as a function of time (adapted from [24]). The solid line represents the quantized drift expected for a Chern number $\mathscr{C} = 1$.

incoherently. Applying a force F_x along the x-direction induces a transverse drift along the y-direction of the center of mass (see Figure 8(b)), as described by

$$y(t) = \frac{4a^2 F_x}{\hbar} \mathscr{C}\, t,$$

where $\mathscr{C}$ is the Chern number of the occupied band. This technique has provided the first experimental evidence of a quantized Chern number in ultracold atomic gases.

2.2.3. *The issue of Floquet heating*

Experiments utilizing shaken optical lattices face a common challenge: the limited duration of coherence due to Floquet heating. This phenomenon arises because the laser-assisted hopping involves a time-dependent potential $V(x,t) \propto \cos(\delta\mathbf{k}\cdot\mathbf{r} - \Delta t)$, where the angular frequency Δ is determined by the energy difference $\hbar\Delta$ between neighbouring wells. While this time modulation prevents the definition of stationary states, the Floquet formalism allows for the characterization of time-periodic eigenstates–eigenstates of the unitary evolution over one modulation period. These states are defined by a quasi-energy that is considered modulo $\hbar\Delta$ (analogous to the quasi-momentum of Bloch states) [27,28].

In the Floquet picture, the notion of ground band no longer makes sense. However, an effective ground band can still be identified when the modulation frequency significantly exceeds the typical tunneling rates and band gaps to higher bands. Despite this, the effective ground band remains coupled to higher bands, which can be brought into resonance by the absorption of quanta of energy $\hbar\Delta$ (see Figure 9(a) and (b)). These detrimental couplings can be mitigated by appropriately selecting the modulation frequency [29]. An additional source of heating arises when considering interacting atoms, which can absorb quanta of the modulation energy during two-body collisional processes [30–33].

These heating processes have not hindered the success of remarkable experiments, including the realization of various types of topological bands and initial studies of strongly interacting systems, as discussed later. However, Floquet heating remains a significant challenge for the

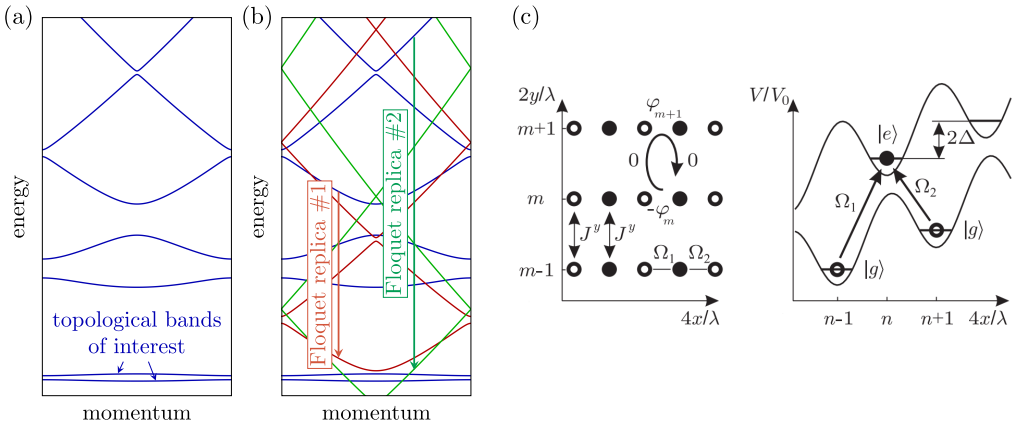

Figure 9. (a) Scheme of a typical bandstructure, with low-energy bands of interest separated in energy with respect to higher dispersive bands. (b) When targeting the bandstructure (a) using time-modulated optical lattices, the modulation frequency Δ gives rise, in a Floquet picture, to an infinite number of replicas separated in energy by integer multiples of the energy quantum $\hbar\Delta$ (two of them are shown in red and green). The bands of interest may become resonantly coupled with higher bands, leading to heating of the system. (c) Reproduction of the scheme of the protocol of Jaksch and Zoller [22], which involves spin flips upon hopping between lattice sites. Such a scheme involves a much higher modulation frequency, which could solve the issue of Floquet heating.

future realization of complex topological states, which require extended experimental timescales for their generation.

Future experiments could address the issue of Floquet heating by employing more complex protocols that utilize an internal degree of freedom of the atom, as originally proposed by Jaksch and Zoller [22] (see also [34]). By ensuring that the laser-assisted tunneling is accompanied by a transition between two internal states (see Figure 9(c)), the modulation frequency $\hbar\Delta$ would become a hyperfine or electronic resonant frequency, which is several orders of magnitude larger than the typical energy scale of motion. In this scenario, an effective static Hamiltonian can be accurately defined, and Floquet heating is not expected to occur.

We also note that an off-resonant laser field coupled to an internal degree of freedom can be utilized to simulate a magnetic field in the continuum. In this scenario, the laser-dressed states become position-dependent due to the spatial variation of the laser electric field. An atom that adiabatically follows a given dressed state experiences a geometrical Berry phase, similar to the Aharonov–Bohm phase experienced by a charged particle in a magnetic field. The group led by Spielman demonstrated the nucleation of quantized vortices in a Bose–Einstein condensate using this technique [35].

2.3. *Synthetic dimensions*

The last technique we discuss involves the concept of synthetic dimensions [36]. In this framework, a quantum Hall system is defined where the xy plane is replaced by a synthetic plane composed of one spatial dimension x and one synthetic dimension [37–39]. The spatial coordinate y is substituted with another degree of freedom, which can be a momentum state or an internal degree of freedom [40,41]. In a well-developed scheme, the discrete projection m of an internal

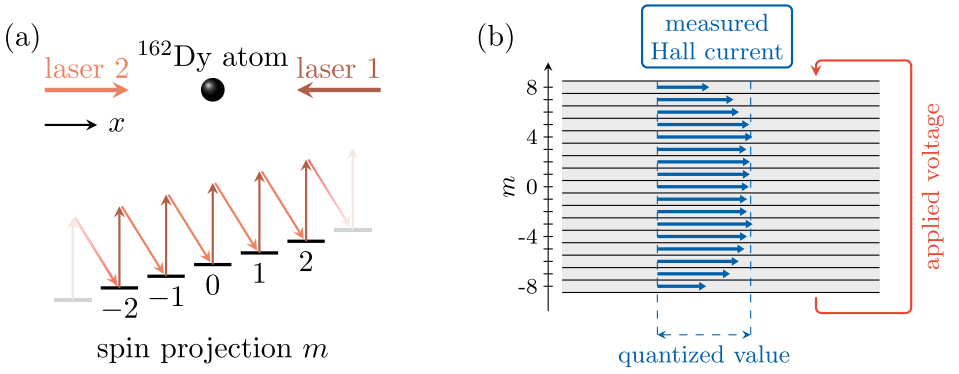

Figure 10. (a) Scheme of the laser configuration used to simulate a magnetic field in a hybrid system involving a spatial dimension x and a synthetic dimension encoded in the spin projection m. The dynamics along m is induced by resonant two-photon optical transitions. An effective magnetic field arises from the velocity kicks that occur along xx during spin transitions. (b) Measured Hall response resolved in magnetic projection m, which is consistent with a quantized value in the bulk of the synthetic dimension.

spin J (with $-J \leq m \leq J$) is utilized [38,39,42]. The dynamics along m is induced by two-photon Raman transitions involving a pair of lasers counter-propagating along x (see Figure 10(a)).

The occurrence of an effective magnetic field arises from the correlated dynamics in the spin projection m and velocity v_x. Specifically, a spin transition $m \to m+1$ is accompanied by a velocity kick $v_x \to v_x - 2\hbar k_{\text{laser}}/M$ due to the momentum exchange with light. This relationship leads to the equation of motion

$$M\dot{v}_x = -2\hbar k_{\text{laser}}\dot{m},$$

which can be interpreted as the dynamics of a charged particle under the influence of a magnetic field

$$M\dot{v}_x = qB\dot{y},$$

where $q = 1$ and $\mathbf{B} = -2\hbar k_{\text{laser}}\mathbf{e}_z$. This effective magnetic field results in a quantum Hall effect, which is evidenced by a quantized transverse response in the bulk of the synthetic dimension [42] (see Figure 10(b)). Synthetic dimensions are particularly advantageous for revealing the occurrence of topological edge modes due to their finite nature [38,39]. They also facilitate the engineering of complex geometries, such as cylinders [43–47] or systems in dimensions greater than three [48,49].

Synthetic dimensions also come with some peculiarities and limitations. First, synthetic dimensions can be limited in size, particularly when encoding them in the internal spin of an atom. Exploring topological effects in the thermodynamic limit then requires using large-spin lanthanide atoms [42]. Alternatively, synthetic dimensions can be encoded in momentum states of an atom [50] or rotational states of a molecule [51], with no fundamental limitation in size.

So far, synthetic dimensions have primarily been employed to engineer various types of topological bands, typically studied in the absence of significant interaction effects. Notable exceptions include two works that reported the observation of non-linear effects in a momentum-state lattice [52] and a universal Hall response in a ladder geometry [53]. More generally, interactions in systems with synthetic dimensions are expected to exhibit a peculiar structure. Since atoms on different synthetic sites can interact, the interactions are anticipated to be of infinite range along

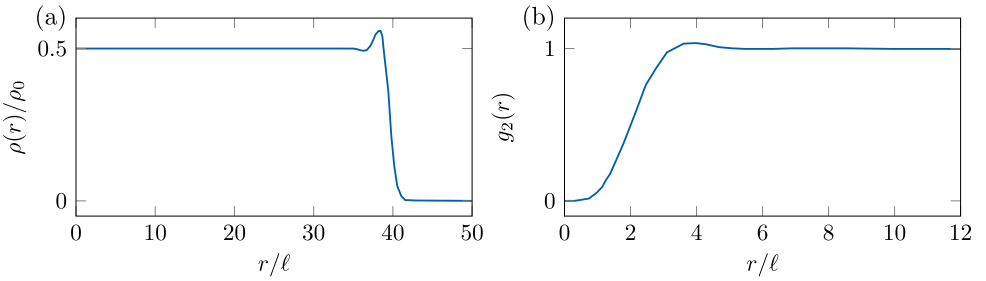

Figure 11. Density profile $\rho(r)$ (a) and correlation function $g_2(r)$ (b) of a bosonic Laughlin state with 400 particles, computed from a Monte Carlo simulation [66].

synthetic dimensions. This characteristic may significantly alter the phenomenology of strongly-interacting topological systems [40,54–59], and the conditions for the occurrence of genuine two-dimensional fractional Hall states in systems with synthetic dimensions remain to be elucidated.

3. Towards fractional quantum Hall states

In the context of a Bose–Einstein condensate, we have primarily considered the many-body ground state where each LLL orbital is filled with a large number of atoms, resulting in a high filling factor $\nu = N_{\rm at}/N_{\rm orb} \gg 1$. In the regime of lower fillings, the many-body system can no longer be described by a macroscopic wavefunction, leading to the emergence of more complex correlations among the particles.

The strongly-correlated regime poses significant challenges for numerical modeling. Even in bosonic systems, the presence of gauge fields results in complex-valued many-body wavefunctions, which introduces a sign problem in Monte Carlo simulations. In many cases, exact diagonalization remains the only viable approach, although it is constrained by the size of the systems that can be studied. Recently, advancements in computational techniques have allowed for the simulation of larger system sizes using methods such as DMRG [60–62] or other tensor network computations [63]. Variational projected entangled-pair states have also been developed to study the bosonic Harper–Hofstadter model in the thermodynamic limit [64].

3.1. *The bosonic Laughlin state*

We focus our discussion on the bosonic Laughlin state at filling factor $\nu = 1/2$, a prominent example of a fractional quantum Hall state [65]. For an ensemble of N particles, the many-body wavefunction is given by

$$\psi_L(z_1, z_2, \ldots, z_N) = \prod_{1\le i<j\le N} (z_i - z_j)^2 \prod_{i=1}^{N} \mathrm{e}^{-|z_i|^2/4\ell^2}.$$

This wavefunction being expressed as a symmetric polynomial of the complex coordinates z_i (aside from a Gaussian factor that we will disregard for simplicity), it belongs to the LLL introduced in Section 1.1. A notable feature of this wavefunction is that it forbids two particles from occupying the same point, as evidenced by the second-order correlation function $g_2(r)$ plotted in Figure 11(b)). This property leads to the remarkable conclusion that the Laughlin state is the exact many-body ground state for zero-range repulsive interactions, a scenario particularly relevant for rotating atomic Bose gases.

Any wavefunction derived by multiplying the Laughlin wavefunction by another symmetric polynomial also exhibits a zero interaction energy. Among this family of degenerate ground

states, the Laughlin state uniquely minimizes the angular momentum projection $m_{\rm tot} = N(N-1)$, effectively leading to a minimal spatial extent centered around $\mathbf{r} = \mathbf{0}$. The maximum (single-particle) angular momentum $m = 2(N-1)$ occupied in the Laughlin state corresponds to a radius $R \simeq 2\sqrt{N}\ell$, which results in an area of $\mathscr{A} = \pi R^2 = 2\times(2\pi\ell)^2 N$. The proportionality $\mathscr{A} \propto N$ reflects the behavior of an incompressible liquid. The bulk density of the Laughlin state is expressed as

$$\bar{\rho} = \rho_0/2, \tag{4}$$

where $\rho_0 = 1/(2\pi\ell^2)$ is the density expected when each orbital is filled with a single particle, akin to a fermionic Hall insulator. In practice, the density is nearly uniform throughout most of the disk $r < R$, with a slight ripple around $r = R$ [66], see Figure 11(a).

Since $\rho_0 \propto B$, the uniform density given in Equation (4) is proportional to the magnetic field strength. According to the Středa formula $\sigma_{xy} = \partial\bar{\rho}/\partial B$, which relates the Hall conductance to the variation of density with respect to the magnetic field [67], we have

$$\sigma_{xy} = \frac{1}{2}\frac{1}{h},$$

i.e. a half-quantized value (we recall our convention of a unit charge $q = 1$). Furthermore, the excitation of density modulations is suppressed in the bulk by a finite energy gap (roughly given by the interaction energy experienced by a pair of atoms in the state $\psi_{m=0}$ [68]).

3.2. *State-of-the art: Laughlin state with 2 particles*

A recent experiment conducted by the group of Greiner has successfully demonstrated the realization of a Laughlin state with just two atoms [69]. In this experiment, the researchers utilized an optical lattice to simulate the Hofstadter model with a flux of $p/q = 1/3$ per plaquette. They confined the dynamics to a 4×4 lattice, resulting in a total flux through the 9 plaquettes amounting to $3\Phi_0$. This configuration corresponds to $N_{\rm orb} = 3$ orbitals in the ground band, which is precisely the number needed to define the Laughlin state.

The interacting two-body ground state was adiabatically prepared by slowly ramping local potential tilts. The resulting state exhibited the expected anti-bunching between the atoms (see Figure 12(a)). Furthermore, by measuring the change in density in response to variations in the artificial magnetic field, they were able to determine a Hall response conductance of $0.6(2)/h$ via the Středa formula. This result is consistent with a half-quantized Hall response (see Figure 12(b)).

A recent preprint from the group of Jochim also reported the realization of a 2-atom Laughlin state composed of a pair of rapidly rotating fermionic atoms [70]. Notably, other platforms have successfully produced two-photon Laughlin states [71,72].

3.3. *Towards larger Laughlin states*

While robust quantization of the Hall conductance only occurs for large enough systems, increasing the number of atoms in a Laughlin droplet remains a significant hurdle. Several approaches can be taken to address this

- Starting with independent one-dimensional chains of atoms, ramping up inter-chain couplings in an adiabatic manner [73].
- A patchwork construction [74], which involves preparing multiple 4×4 plaquettes, each containing 2 atoms in a Laughlin state, and then adiabatically coupling these plaquettes together.

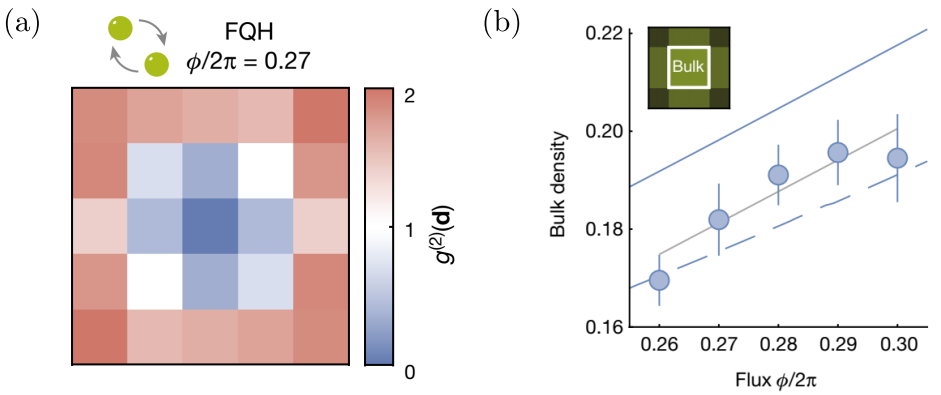

Figure 12. Correlation function $g_2(\mathrm{d})$ measured for a 2-particle Laughlin state in [69] (b) Variation of the density with magnetic flux measured in the same system, consistent with a half-quantized Hall conductance.

- By adjusting a parameter that controls a phase transition from a non-topological to a topological band, similar to methods using local energy offsets [24], one can transition from a trivial phase (like a Bose superfluid) to a Laughlin state [62].

In these methods, maintaining an adiabatic process is crucial for achieving a low-entropy Laughlin state. The importance of the adiabatic path was highlighted in earlier proposals for creating small Laughlin states in rotating systems [75]. However, as the number of atoms increases, it becomes increasingly difficult to maintain adiabatic conditions.

Another potential approach is to create a more complex system with a central region hosting a Laughlin droplet surrounded by a large reservoir in a gapless non-topological phase [76]. By tuning the energy of the reservoir, it may be possible to transfer entropy from the central region to the reservoir, resulting in a low-entropy Laughlin droplet. This technique has been successfully used in lattice Fermi gases to produce antiferromagnets with long-range magnetic order [77].

Finally, we mention proposals for preparing topological many-body states using dissipative dynamics [78,79], for instance fractional Hall states by pumping interacting bosons into the lowest Chern band of a topological lattice [80].

3.4. *Probing long-range entanglement*

In contrast to an integer quantum Hall phase, a fractional Hall state exhibits long-ranged entanglement associated with what is known as topological order [81]. This topological order is characterized by the existence of degenerate many-body ground states in a toroidal geometry that cannot be distinguished using local observables. However, this property poses challenges for experiments, as implementing periodic boundary conditions can be difficult.

Topological order can be more easily revealed by analyzing long-range entanglement through the entanglement entropy $S_A = -\mathrm{Tr}(\rho_A \log \rho_A)$ upon spatial partition of the system between two subregions A and B (where ρ_A is the reduced density matrix obtained by tracing out the B subregion). For a partition with a perimeter L, systems with short-range entanglement follow the area law, scaling linearly with L according to $S_A(L) = \alpha L + o(1)$ [82], whereas systems with topological order are expected to modify this law to $S_A(L) = \alpha L - \gamma + o(1)$. The subleading term γ, known as the topological shift, quantifies a global entanglement feature that persists over long distances [83].

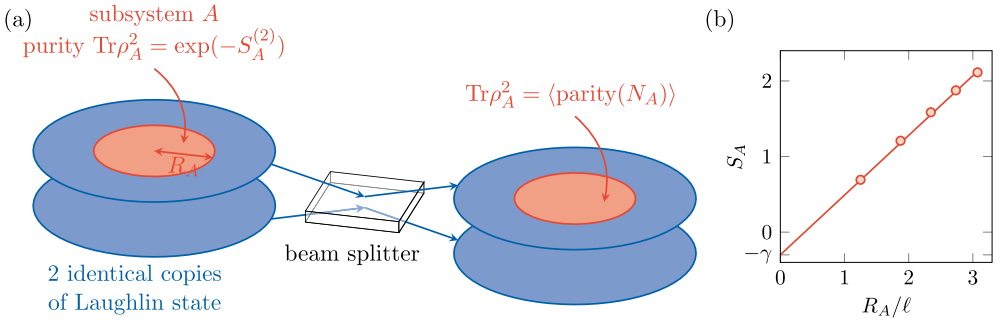

Figure 13. (a) Scheme of the method for measuring the (Renyi) entanglement entropy of a subregion A within a many-body system. The process involves interfering two identical copies of the system using a 50/50 beam splitter. The purity of the reduced density matrix ρ_A can then be determined from the mean parity of the atom count in region A [84,85]. (b) Expected variation of the (von Neumann) entanglement entropy S_A as a function of the radius R_A of subregion A. The y-intercept of the linear fit represents the entanglement entropy γ (from [88]).

The group led by Greiner has successfully measured the Renyi entanglement entropy defined as $S_A^{(2)} = -\log \mathrm{Tr}(\rho_A^2)$, using a protocol based on many-body interference between two copies of a many-body system [84,85] (see Figure 13(a)). In this approach, two copies 1 and 2 of a bosonic many-body state undergo a local beam-splitter operation $|1\rangle \to (|1\rangle + |2\rangle)/\sqrt{2}$ and $|2\rangle \to (|1\rangle - |2\rangle)/\sqrt{2}$. The purity of the system reduced to subregion A is linked to the mean parity of the number of particles $N_A^{(1)}$ found in region A of system 1 after the splitting as

$$\mathrm{Tr}(\rho_A^2) = \langle \mathrm{Parity}(N_A^{(1)})\rangle.$$

If the original many-body state is pure, an even number of atoms is expected in system 1, similar to the Hanbury Brown and Twiss effect. As the size of A increases from zero, the mean parity should quiclky drop to zero on a lengthscale ℓ. Taking the logarithm gives the Renyi entropy, whose scaling with L can reveal the topological shift γ. Numerical simulations on small Laughlin droplets confirm this scenario [86–88] (see Figure 13(b)).

3.5. *Anyonic quasi-hole excitations*

A key feature of fractional quantum Hall states is the unique nature of their elementary excitations. We recall that a wavefunction $\psi(z_1, z_2, \ldots, z_N) = P(z_1, z_2, \ldots, z_N)\psi_L(z_1, z_2, \ldots, z_N)$, where P is a symmetric polynomial, exhibits zero interaction energy and is therefore degenerate with the Laughlin ground state. A polynomial P with a degree less than the number of particles corresponds to edge excitations of the Laughlin droplet. Here, we focus on a bulk excitation, known as a quasi-hole excitation, represented by

$$\psi_\eta(z_1, z_2, \ldots, z_N) = \prod_{i=1}^{N}(z_i - \eta)\psi_L(z_1, z_2, \ldots, z_N).$$

It exhibits a density hole at $z = \eta$, corresponding to a deficit of 1/2 particle (see Figure 14(b)). This can be understood by considering two quasi-holes at the same point, leading to the wavefunction

$$\psi_{\eta,\eta}(z_1, z_2, \ldots, z_N) = \prod_{i=1}^{N}(z_i - \eta)^2\psi_L(z_1, z_2, \ldots, z_N).$$

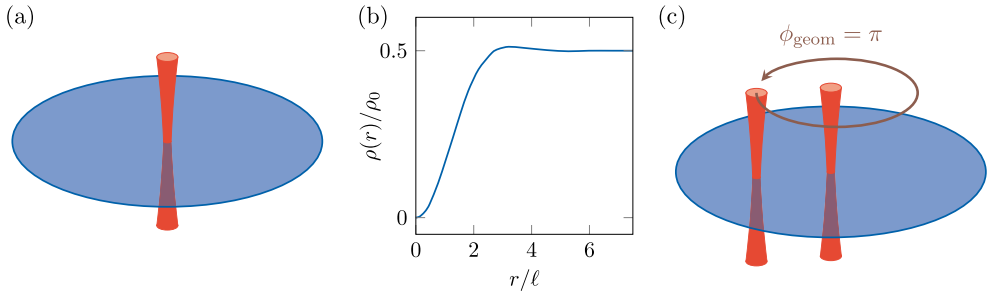

Figure 14. (a) Scheme of the protocol used to nucleate a quasi-hole excitation by focusing a laser beam producing a repulsive potential. (b) Density profile of a Laughlin state with a quasi-hole excitation at $r = 0$ (from [89]). The atom number deficit corresponds to a fractional charge of $1/2$ atom, and the r.m.s. size of the hole is linked with the quasi-hole spin $S = 1/4$. (c) Scheme of the braiding operation by moving adiabatically one quasi-hole around another, which gives rise to a geometrical phase $\phi_{\rm geom} = 2S(2\pi) = \pi$.

It can be identified with the state obtained by removing from a Laughlin wavefunction of $(N+1)$ particles a single atom at $z_{N+1} = \eta$.

In practice, a quasi-hole state can be generated by applying a repulsive laser beam focused at $z = \eta$ [90] (see Figure 14(a)). This technique is already well-established for injecting and controlling quantum vortices in Bose–Einstein condensates [91,92].

Beyond the fractional charge, the quasi-hole density profile provides further insights [93]. The relationship between the mean square radius and angular momentum [94] indicates that the size of the quasi-hole is linked to its angular momentum, according to

$$\delta L_z = \int \mathrm{d}^2 z \left(\frac{|z-\eta|^2}{2\ell^2} - 1 \right) (\rho_\eta(z) - \bar{\rho}).$$

This excess angular momentum can be interpreted as the internal spin $S = \delta L_z$ of the quasi-hole [89]. For the bosonic Laughlin state, numerical studies suggest $S = 1/4$. This fractional spin challenges the conventional understanding of half-integer and integer spins for fermions and bosons, respectively. According to the spin-statistics theorem, this hints at the existence of a fractional statistical phase, leading to the term anyons for such quasi-particles [95]. Real-space probes of quasi-hole excitations can also be generalized to Chern insulators in lattice systems [96].

3.6. *Braiding of anyonic excitations*

The fractional statistical phase is defined as the geometrical phase acquired by the system upon an exchange of two particles. To probe this statistical phase, two key requirements must be met (i) the ability to create and spatially manipulate quasiholes, which can be achieved using focused laser beams (see Figure 14(c)). When a quasihole encircles another, the many-body system acquires a statistical phase given by $\phi_{\rm geom} = 2S(2\pi) = \pi$. (ii) an interferometric protocol to reveal the value of this phase. We do not discuss this point here and refer to the first proposal for a statistical phase interferometer in the context of cold atomic gases, by Paredes et al. [97].

Successful measurement of the statistical phase hinges on minimizing various imperfections. First, the geometrical phase should not be significantly affected by a dynamical phase that may arise during the adiabatic braiding process. This dynamical phase can occur if there is cross-talk between the quasiholes when they are too close together or if they are positioned near

the confining edge potential. To keep dynamical phases small, uncontrolled energy offsets must be maintained well below the bulk excitation gap. Second, the Laughlin droplet must be prepared with very low residual entropy to ensure that the average number of thermal quasiholes remains negligible over the area encircled by the quasiholes during the braiding operation. These stringent requirements impose significant constraints on the control over the system, making the measurement quite challenging.

3.7. *Extension to other fractional quantum Hall states*

So far, our discussion has focused on the bosonic Laughlin state at filling $\nu = 1/2$. This focus is motivated by the fact that the Laughlin state emerges as the exact many-body ground state for short-range binary interactions, making it the most experimentally accessible fractional quantum Hall state in quantum gas systems. Other fractional quantum Hall states could also be realized using more sophisticated experimental protocols. While each fractional Hall state is characterized by a unique topological order, certain key properties—such as topological entropy or the existence of fractionalized quasi-particles—can be probed using protocols similar to those developed for the Laughlin state.

Among the various fractional Hall states, the bosonic Moore-Read/Pfaffian state, which occurs at filling $\nu = 1$, is particularly noteworthy due to its exotic properties. This state involves the pairing of bosonic particles and is characterized by three-body antibunching. As a result, it could be stabilized in the presence of three-body repulsive interactions [98], although engineering such interactions remains a significant experimental challenge. Alternatively, it has been proposed that the Pfaffian state could be stabilized through strong three-body dissipation [99] or by carefully tuning two-body interactions [100]. The Pfaffian state is especially intriguing because its elementary excitations exhibit non-Abelian exchange statistics [101]. Demonstrating non-Abelian braiding of these excitations—a critical step toward realizing topological quantum computing [102]—remains one of the most ambitious challenges in experimental physics across platforms.

4. Conclusion

In this proceedings, we have discussed the current status of simulating quantum Hall physics using ultracold atomic gases. Various techniques have been explored to replicate the effects of a magnetic field on charged particles, including rotating gases, lattice systems, and synthetic dimensions. While the realization of topological bands is well-established at the single-particle level, achieving strongly-interacting topological systems remains a significant challenge. Recent advancements, leveraging a high degree of control over local potentials and individual particles, have shown promising progress toward realizing fractional quantum Hall systems in ultracold atomic gases.

While our focus has been primarily on the quantum Hall effect, the field of ultracold atomic gases has also seen the emergence of diverse topological systems, such as 1D SSH chains [103], spin-orbit coupled systems [104] and 3D Weyl semi-metals [105]. The exploration of interacting gases within these topological band structures opens up exciting possibilities for discovering a wide range of intriguing strongly-correlated systems.

Declaration of interests

The authors do not work for, advise, own shares in, or receive funds from any organization that could benefit from this article, and have declared no affiliations other than their research organizations.

Acknowledgements

The author acknowledges fruitful discussions with Jean Dalibard while preparing the talk at the Institut Henri Poincaré. The author also acknowledges support from European Union (grant TOPODY 756722 from the European Research Council) and Institut Universitaire de France.

References

[1] K. v. Klitzing, G. Dorda and M. Pepper, "New method for high-accuracy determination of the fine-structure constant based on quantized Hall resistance", *Phys. Rev. Lett.* **45** (1980), pp. 494–497.

[2] L. D. Landau and E. M. Lifshitz, *Course of Theoretical Physics Vol 3 Quantum Mechanics*, Pergamon Press: London, 1958.

[3] B. I. Halperin, "Quantized Hall conductance, current-carrying edge states, and the existence of extended states in a two-dimensional disordered potential", *Phys. Rev. B* **25** (1982), pp. 2185–2190.

[4] Y. Castin, Z. Hadzibabic, S. Stock, J. Dalibard and S. Stringari, "Quantized vortices in the ideal Bose gas: a physical realization of random polynomials", *Phys. Rev. Lett.* **96** (2006), article no. 040405.

[5] R. B. Laughlin, "Quantized Hall conductivity in two dimensions", *Phys. Rev. B* **23** (1981), pp. 5632–5633.

[6] O. M. Corbino, "Azioni Elettromagnetiche Doyute Agli Ioni dei Metalli Deviati Dalla Traiettoria Normale per Effetto di un Campo", *Nuovo Cimento* **1** (1911), pp. 397–420.

[7] P. G. Harper, "Single band motion of conduction electrons in a uniform magnetic field", *Proc. Phys. Soc. A* **68** (1955), pp. 874–878.

[8] D. R. Hofstadter, "Energy levels and wave functions of Bloch electrons in rational and irrational magnetic fields", *Phys. Rev. B* **14** (1976), pp. 2239–2249.

[9] N. R. Cooper, J. Dalibard and I. B. Spielman, "Topological bands for ultracold atoms", *Rev. Mod. Phys.* **91** (2019), article no. 015005.

[10] F. D. M. Haldane, "Model for a quantum Hall effect without Landau levels: condensed-matter realization of the "Parity Anomaly"", *Phys. Rev. Lett.* **61** (1988), pp. 2015–2018.

[11] K. W. Madison, F. Chevy, W. Wohlleben and J. Dalibard, "Vortex formation in a stirred Bose–Einstein condensate", *Phys. Rev. Lett.* **84** (2000), pp. 806–809.

[12] K. W. Madison, F. Chevy, W. Wohlleben and J. Dalibard, "Vortices in a stirred Bose–Einstein condensate", *J. Mod. Opt.* **47** (2000), pp. 2715–2723.

[13] A. A. Abrikosov, "On the magnetic properties of superconductors of the second group", *Sov. Phys. - JETP* **5** (1957), pp. 1174–1182.

[14] W. H. Kleiner, L. M. Roth and S. H. Autler, "Bulk solution of Ginzburg–Landau equations for type II superconductors: upper critical field region", *Phys. Rev.* **133** (1964), A1226–A1227.

[15] J. R. Abo-Shaeer, C. Raman, J. M. Vogels and W. Ketterle, "Observation of vortex lattices in Bose–Einstein condensates", *Science* **292** (2001), pp. 476–479.

[16] V. Bretin, S. Stock, Y. Seurin and J. Dalibard, "Fast rotation of a Bose–Einstein condensate", *Phys. Rev. Lett.* **92** (2004), article no. 050403.

[17] V. Schweikhard, I. Coddington, P. Engels, V. P. Mogendorff and E. A. Cornell, "Rapidly rotating Bose–Einstein condensates in and near the lowest Landau level", *Phys. Rev. Lett.* **92** (2004), article no. 040404.

[18] R. J. Fletcher, A. Shaffer, C. C. Wilson, P. B. Patel, Z. Yan, V. Crépel, B. Mukherjee and M. W. Zwierlein, "Geometric squeezing into the lowest Landau level", *Science* **372** (2021), pp. 1318–1322.

[19] R. Yao, S. Chi, B. Mukherjee, A. Shaffer, M. Zwierlein and R. J. Fletcher, "Observation of chiral edge transport in a rapidly-Rotating quantum gas", *Nat. Phys.* **20** (2024), pp. 1726–1731.

[20] B. Mukherjee, A. Shaffer, P. B. Patel, Z. Yan, C. C. Wilson, V. Crépel, R. J. Fletcher and M. Zwierlein, "Crystallization of bosonic quantum Hall states in a rotating quantum gas", *Nature* **601** (2022), pp. 58–62.

[21] C. Gross and I. Bloch, "Quantum simulations with ultracold atoms in optical lattices", *Science* **357** (2017), pp. 995–1001.

[22] D. Jaksch and P. Zoller, "Creation of effective magnetic fields in optical lattices: the Hofstadter butterfly for cold neutral atoms", *New J. Phys.* **5** (2003), article no. 56.

[23] M. Aidelsburger, M. Atala, M. Lohse, J. T. Barreiro, B. Paredes and I. Bloch, "Realization of the Hofstadter Hamiltonian with ultracold atoms in optical lattices", *Phys. Rev. Lett.* **111** (2013), article no. 185301.

[24] M. Aidelsburger, M. Lohse, C. Schweizer, et al., "Measuring the Chern number of Hofstadter bands with ultracold bosonic atoms", *Nat. Phys.* **11** (2015), pp. 162–166.

[25] H. Miyake, G. A. Siviloglou, C. J. Kennedy, W. C. Burton and W. Ketterle, "Realizing the Harper Hamiltonian with laser-assisted tunneling in optical lattices", *Phys. Rev. Lett.* **111** (2013), article no. 185302.

[26] G. Jotzu, M. Messer, R. Desbuquois, M. Lebrat, T. Uehlinger, D. Greif and T. Esslinger, "Experimental realization of the topological Haldane model with ultracold fermions", *Nature* **515** (2014), pp. 237–240.
[27] M. Holthaus, "Floquet engineering with quasienergy bands of periodically driven optical lattices", *J. Phys. B: At. Mol. Opt. Phys.* **49** (2015), article no. 013001.
[28] A. Eckardt, "Colloquium: atomic quantum gases in periodically driven optical lattices", *Rev. Mod. Phys.* **89** (2017), article no. 011004.
[29] M. Weinberg, C. Ölschläger, C. Sträter, S. Prelle, A. Eckardt, K. Sengstock and J. Simonet, "Multiphoton interband excitations of quantum gases in driven optical lattices", *Phys. Rev. A* **92** (2015), article no. 043621.
[30] M. Reitter, J. Näger, K. Wintersperger, C. Sträter, I. Bloch, A. Eckardt and U. Schneider, "Interaction dependent heating and atom loss in a periodically driven optical lattice", *Phys. Rev. Lett.* **119** (2017), article no. 200402.
[31] T. Boulier, J. Maslek, M. Bukov, et al., "Parametric heating in a 2D periodically driven bosonic system: beyond the weakly interacting regime", *Phys. Rev. X* **9** (2019), article no. 011047.
[32] K. Wintersperger, M. Bukov, J. Näger, et al., "Parametric instabilities of interacting bosons in periodically driven 1D optical lattices", *Phys. Rev. X* **10** (2020), article no. 011030.
[33] K. Viebahn, J. Minguzzi, K. Sandholzer, A.-S. Walter, M. Sajnani, F. Görg and T. Esslinger, "Suppressing dissipation in a Floquet–Hubbard system", *Phys. Rev. X* **11** (2021), article no. 011057.
[34] F. Gerbier and J. Dalibard, "Gauge fields for ultracold atoms in optical superlattices", *New J. Phys.* **12** (2010), article no. 033007.
[35] Y.-J. Lin, R. L. Compton, K. Jiménez-García, J. V. Porto and I. B. Spielman, "Synthetic magnetic fields for ultracold neutral atoms", *Nature* **462** (2009), pp. 628–632.
[36] O. Boada, A. Celi, J. I. Latorre and M. Lewenstein, "Quantum simulation of an extra dimension", *Phys. Rev. Lett.* **108** (2012), article no. 133001.
[37] A. Celi, P. Massignan, J. Ruseckas, N. Goldman, I. B. Spielman, G. Juzeliūnas and M. Lewenstein, "Synthetic gauge fields in synthetic dimensions", *Phys. Rev. Lett.* **112** (2014), article no. 043001.
[38] M. Mancini, G. Pagano, G. Cappellini, et al., "Observation of Chiral edge states with neutral fermions in synthetic hall ribbons", *Science* **349** (2015), pp. 1510–1513.
[39] B. K. Stuhl, H.-I. Lu, L. M. Aycock, D. Genkina and I. B. Spielman, "Visualizing edge states with an atomic Bose gas in the quantum Hall regime", *Science* **349** (2015), pp. 1514–1518.
[40] T. Ozawa and H. M. Price, "Topological quantum matter in synthetic dimensions", *Nat. Rev. Phys.* **1** (2019), pp. 349–357.
[41] A. Fabre and S. Nascimbene, "Atomic topological quantum matter using synthetic dimensions", *Europhys. Lett.* **145** (2024), article no. 65001.
[42] T. Chalopin, T. Satoor, A. Evrard, V. Makhalov, J. Dalibard, R. Lopes and S. Nascimbene, "Probing Chiral edge dynamics and bulk topology of a synthetic Hall system", *Nat. Phys.* **16** (2020), pp. 1017–1021.
[43] J. H. Han, J. H. Kang and Y. Shin, "Band gap closing in a synthetic Hall tube of neutral fermions", *Phys. Rev. Lett.* **122** (2019), article no. 065303.
[44] Y. Yan, S.-L. Zhang, S. Choudhury and Q. Zhou, "Emergent periodic and quasiperiodic lattices on surfaces of synthetic Hall tori and synthetic Hall cylinders", *Phys. Rev. Lett.* **123** (2019), article no. 260405.
[45] X.-W. Luo, J. Zhang and C. Zhang, "Tunable flux through a synthetic Hall tube of neutral fermions", *Phys. Rev. A* **102** (2020), article no. 063327.
[46] Q.-Y. Liang, D. Trypogeorgos, A. Valdés-Curiel, J. Tao, M. Zhao and I. B. Spielman, "Coherence and decoherence in the Harper–Hofstadter model", *Phys. Rev. Res.* **3** (2021), article no. 023058.
[47] A. Fabre, J.-B. Bouhiron, T. Satoor, R. Lopes and S. Nascimbene, "Laughlin's topological charge pump in an atomic Hall cylinder", *Phys. Rev. Lett.* **128** (2022), article no. 173202.
[48] M. Lohse, C. Schweizer, H. M. Price, O. Zilberberg and I. Bloch, "Exploring 4D quantum Hall physics with a 2D topological charge pump", *Nature* **553** (2018), pp. 55–58.
[49] J.-B. Bouhiron, A. Fabre, Q. Liu, Q. Redon, N. Mittal, T. Satoor, R. Lopes and S. Nascimbene, "Realization of an atomic quantum Hall system in four dimensions", *Science* **384** (2024), pp. 223–227.
[50] F. A. An, E. J. Meier, J. Ang'ong'a and B. Gadway, "Correlated dynamics in a synthetic lattice of momentum states", *Phys. Rev. Lett.* **120** (2018), article no. 040407.
[51] B. Sundar, B. Gadway and K. R. A. Hazzard, "Synthetic dimensions in ultracold polar molecules", *Sci. Rep.* **8** (2018), article no. 3422.
[52] F. A. An, B. Sundar, J. Hou, X.-W. Luo, E. J. Meier, C. Zhang, K. R. A. Hazzard and B. Gadway, "Nonlinear dynamics in a synthetic momentum-state lattice", *Phys. Rev. Lett.* **127** (2021), article no. 130401.
[53] T.-W. Zhou, G. Cappellini, D. Tusi, et al., "Observation of universal Hall response in strongly interacting fermions", *Science* **381** (2023), pp. 427–430.
[54] S. Barbarino, L. Taddia, D. Rossini, L. Mazza and R. Fazio, "Magnetic crystals and helical liquids in alkaline-earth fermionic gases", *Nat. Commun.* **6** (2015), pp. 1–9.

[55] E. Cornfeld and E. Sela, "Chiral currents in one-dimensional fractional quantum Hall states", *Phys. Rev. B* **92** (2015), article no. 115446.
[56] M. Łącki, H. Pichler, A. Sterdyniak, A. Lyras, V. E. Lembessis, O. Al-Dossary, J. C. Budich and P. Zoller, "Quantum Hall physics with cold atoms in cylindrical optical lattices", *Phys. Rev. A* **93** (2016), article no. 013604.
[57] S. Barbarino, L. Taddia, D. Rossini, L. Mazza and R. Fazio, "Synthetic gauge fields in synthetic dimensions: interactions and chiral edge modes", *New J. Phys.* **18** (2016), article no. 035010.
[58] T. Bilitewski and N. R. Cooper, "Synthetic dimensions in the strong-coupling limit: supersolids and pair superfluids", *Phys. Rev. A* **94** (2016), article no. 023630.
[59] J. Jünemann, A. Piga, S.-J. Ran, M. Lewenstein, M. Rizzi and A. Bermudez, "Exploring interacting topological insulators with ultracold atoms: the synthetic Creutz–Hubbard model", *Phys. Rev. X* **7** (2017), article no. 031057.
[60] M. P. Zaletel, R. S. K. Mong and F. Pollmann, "Topological characterization of fractional quantum Hall ground states from microscopic Hamiltonians", *Phys. Rev. Lett.* **110** (2013), article no. 236801.
[61] J. Motruk, M. P. Zaletel, R. S. K. Mong and F. Pollmann, "Density matrix renormalization group on a cylinder in mixed real and momentum space", *Phys. Rev. B* **93** (2016), article no. 155139.
[62] J. Motruk and F. Pollmann, "Phase transitions and adiabatic preparation of a fractional Chern insulator in a Boson cold-atom model", *Phys. Rev. B* **96** (2017), article no. 165107.
[63] M. Gerster, M. Rizzi, P. Silvi, M. Dalmonte and S. Montangero, "Fractional quantum Hall effect in the interacting hofstadter model via tensor networks", *Phys. Rev. B* **96** (2017), article no. 195123.
[64] E. L. Weerda and M. Rizzi, "Fractional quantum Hall states with variational projected entangled-pair states: a study of the bosonic Harper–Hofstadter model", *Phys. Rev. B* **109** (2024), article no. L241117.
[65] R. B. Laughlin, "Anomalous quantum Hall effect: an incompressible quantum fluid with fractionally charged excitations", *Phys. Rev. Lett.* **50** (1983), pp. 1395–1398.
[66] O. Ciftja, "Monte Carlo study of Bose Laughlin wave function for filling factors 1/2, 1/4 and 1/6", *Europhys. Lett.* **74** (2006), p. 486.
[67] P. Streda, "Theory of quantised Hall conductivity in two dimensions", *J. Phys. C: Solid State Phys.* **15** (1982), p. L717.
[68] N. Regnault and T. Jolicoeur, "Quantum Hall fractions in rotating Bose–Einstein condensates", *Phys. Rev. Lett.* **91** (2003), article no. 030402.
[69] J. Léonard, S. Kim, J. Kwan, P. Segura, F. Grusdt, C. Repellin, N. Goldman and M. Greiner, "Realization of a fractional quantum Hall state with ultracold atoms", *Nature* **619** (2023), pp. 495–499.
[70] P. Lunt, P. Hill, J. Reiter, P. M. Preiss, M. Gaka and S. Jochim, "Realization of a Laughlin state of two rapidly rotating fermions", *Phys. Rev. Lett.* **133** (2024), article no. 253401.
[71] L. W. Clark, N. Schine, C. Baum, N. Jia and J. Simon, "Observation of Laughlin states made of light", *Nature* **582** (2020), pp. 41–45.
[72] C. Wang, F.-M. Liu, M.-C. Chen, et al., "Realization of fractional quantum Hall state with interacting photons", *Science* **384** (2024), pp. 579–584.
[73] Y.-C. He, F. Grusdt, A. Kaufman, M. Greiner and A. Vishwanath, "Realizing and adiabatically preparing bosonic integer and fractional quantum Hall states in optical lattices", *Phys. Rev. B* **96** (2017), article no. 201103.
[74] F. A. Palm, J. Kwan, B. Bakkali-Hassani, M. Greiner, U. Schollwöck, N. Goldman and F. Grusdt, "Growing extended Laughlin states in a quantum gas microscope: a patchwork construction", *Phys. Rev. Res.* **6** (2024), article no. 013198.
[75] M. Popp, B. Paredes and J. I. Cirac, "Adiabatic path to fractional quantum Hall states of a few bosonic atoms", *Phys. Rev. A* **70** (2004), article no. 053612.
[76] B. Wang, M. Aidelsburger, J. Dalibard, A. Eckardt and N. Goldman, "Cold-atom elevator: from edge-state injection to the preparation of fractional Chern insulators", *Phys. Rev. Lett.* **132** (2024), article no. 163402.
[77] A. Mazurenko, C. S. Chiu, G. Ji, et al., "A cold-atom Fermi–Hubbard antiferromagnet", *Nature* **545** (2017), pp. 462–466.
[78] S. Diehl, E. Rico, M. A. Baranov and P. Zoller, "Topology by dissipation in atomic quantum wires", *Nat. Phys.* **7** (2011), pp. 971–977.
[79] J. C. Budich, P. Zoller and S. Diehl, "Dissipative preparation of Chern insulators", *Phys. Rev. A* **91** (2015), article no. 042117.
[80] Z. Liu, E. J. Bergholtz and J. C. Budich, "Dissipative preparation of fractional Chern insulators", *Phys. Rev. Res.* **3** (2021), article no. 043119.
[81] X. G. Wen, "Topological orders in rigid states", *Int. J. Mod. Phys. B* **04** (1990), pp. 239–271.
[82] J. Eisert, M. Cramer and M. B. Plenio, "*Colloquium*: area laws for the entanglement entropy", *Rev. Mod. Phys.* **82** (2010), pp. 277–306.
[83] A. Kitaev and J. Preskill, "Topological entanglement entropy", *Phys. Rev. Lett.* **96** (2006), article no. 110404.
[84] A. J. Daley, H. Pichler, J. Schachenmayer and P. Zoller, "Measuring entanglement growth in quench dynamics of bosons in an optical lattice", *Phys. Rev. Lett.* **109** (2012), article no. 020505.

[85] R. Islam, R. Ma, P. M. Preiss, M. Eric Tai, A. Lukin, M. Rispoli and M. Greiner, "Measuring entanglement entropy in a quantum many-body system", *Nature* **528** (2015), pp. 77–83.
[86] O. S. Zozulya, M. Haque, K. Schoutens and E. H. Rezayi, "Bipartite entanglement entropy in fractional quantum Hall states", *Phys. Rev. B* **76** (2007), article no. 125310.
[87] M. Haque, O. Zozulya and K. Schoutens, "Entanglement entropy in fermionic Laughlin states", *Phys. Rev. Lett.* **98** (2007), article no. 060401.
[88] A. G. Morris and D. L. Feder, "Topological entropy of quantum Hall states in rotating Bose gases", *Phys. Rev. A* **79** (2009), article no. 013619.
[89] T. Comparin, A. Opler, E. Macaluso, A. Biella, A. P. Polychronakos and L. Mazza, "Measurable fractional spin for quantum Hall quasiparticles on the disk", *Phys. Rev. B* **105** (2022), article no. 085125.
[90] B. Wang, X. Dong and A. Eckardt, "Measurable signatures of bosonic fractional Chern insulator states and their fractional excitations in a quantum-gas microscope", *SciPost Phys.* **12** (2022), article no. 095.
[91] E. C. Samson, K. E. Wilson, Z. L. Newman and B. P. Anderson, "Deterministic creation, pinning, and manipulation of quantized vortices in a Bose–Einstein condensate", *Phys. Rev. A* **93** (2016), article no. 023603.
[92] W. J. Kwon, G. Del Pace, K. Xhani, L. Galantucci, A. Muzi Falconi, M. Inguscio, F. Scazza and G. Roati, "Sound emission and annihilations in a programmable quantum vortex collider", *Nature* **600** (2021), pp. 64–69.
[93] E. Macaluso, T. Comparin, L. Mazza and I. Carusotto, "Fusion channels of non-Abelian anyons from angular-momentum and density-profile measurements", *Phys. Rev. Lett.* **123** (2019), article no. 266801.
[94] T.-L. Ho and E. J. Mueller, "Rotating spin-1 Bose clusters", *Phys. Rev. Lett.* **89** (2002), article no. 050401.
[95] F. Wilczek, "Quantum mechanics of fractional-spin particles", *Phys. Rev. Lett.* **49** (1982), pp. 957–959.
[96] R. O. Umucalılar, "Real-space probe for lattice quasiholes", *Phys. Rev. A* **98** (2018), article no. 063629.
[97] B. Paredes, P. Fedichev, J. I. Cirac and P. Zoller, "1/2-anyons in small atomic Bose–Einstein condensates", *Phys. Rev. Lett.* **87** (2001), article no. 010402.
[98] M. Greiter, X.-G. Wen and F. Wilczek, "Paired Hall state at half filling", *Phys. Rev. Lett.* **66** (1991), pp. 3205–3208.
[99] M. Roncaglia, M. Rizzi and J. I. Cirac, "Pfaffian state generation by strong three-body dissipation", *Phys. Rev. Lett.* **104** (2010), article no. 096803.
[100] F. A. Palm, M. Buser, J. Léonard, M. Aidelsburger, U. Schollwöck and F. Grusdt, "Bosonic Pfaffian state in the Hofstadter–Bose–Hubbard model", *Phys. Rev. B* **103** (2021), article no. L161101.
[101] G. Moore and N. Read, "Nonabelions in the fractional quantum Hall effect", *Nucl. Phys. B* **360** (1991), pp. 362–396.
[102] C. Nayak, S. H. Simon, A. Stern, M. Freedman and S. Das Sarma, "Non-Abelian anyons and topological quantum computation", *Rev. Mod. Phys.* **80** (2008), pp. 1083–1159.
[103] M. Atala, M. Aidelsburger, J. T. Barreiro, D. Abanin, T. Kitagawa, E. Demler and I. Bloch, "Direct measurement of the Zak phase in topological bloch bands", *Nat. Phys.* **9** (2013), pp. 795–800.
[104] Y.-J. Lin, K. Jiménez-García and I. B. Spielman, "Spin–orbit-coupled Bose–Einstein condensates", *Nature* **471** (2011), pp. 83–86.
[105] Z.-Y. Wang, X.-C. Cheng, B.-Z. Wang, et al., "Realization of an ideal Weyl semimetal band in a quantum gas with 3D spin–orbit coupling", *Science* **372** (2021), pp. 271–276.